Journal of Applied Polymer Science

Preparation and Adsorption Behaviors of Ethylene Diamine Tetraacetic Acid Modified Zwitterionic Hybrid Materials

Donglin Zhao,[1] Chen Liu,[1] Junsheng Liu,[2] Jing Zou,[2] Meng Li[2]

[1]School of Materials and Chemical Engineering, Anhui Jianzhu University, 292 Ziyun Road, Hefei Economic and Technological Development Zone, Hefei 230601, China

[2]Key Laboratory of Membrane Materials and Processes, Department of Chemical and Materials Engineering, Hefei University, 99 Jinxiu Road, Hefei Economic and Technological Development Zone, Hefei 230601, China

Correspondence to: J. Liu (E-mail: jsliu@hfuu.edu.cn) or D. Zhao (E-mail: zhaodlin@126.com)

ABSTRACT: Novel ethylene diamine tetraacetic acid (EDTA)-modified zwitterionic hybrid materials were prepared via a sol–gel process. Their adsorption performances for Pb^{2+} ions were examined. Fourier transform infrared spectroscopy confirmed the reaction products. Thermogravimetric analysis revealed that the thermal stability of these hybrid materials could reach 200°C. Differential scanning calorimetry measurement showed that the addition of titanium butoxide could impact the crystallization transformation of these materials. Field emission scanning electron microscopy images showed that EDTA modification induced a decrease in the particle size. Adsorption experiments demonstrated that the optimal initial pH was 5. Moreover, we observed that the adsorptions for Pb^{2+} ions followed the Lagergren pseudo-second-order kinetic model, intraparticle diffusion, and Langmuir isotherm model. In addition, we found that the maximal Langmuir constant was 0.86 mmol/g. The negative Gibbs free energy values suggested that Pb^{2+} adsorption onto these samples was spontaneous in nature. The desorption experiment indicated that these samples could be recovered with aqueous HCl solution as a desorbent. These results suggest that the synthesized EDTA-modified zwitterionic hybrid materials are promising adsorbents that could be used to separate and recover heavy-metal ions from polluted wastewater. © 2013 Wiley Periodicals, Inc. J. Appl. Polym. Sci. **2014**, *131*, 39801.

KEYWORDS: adsorption; kinetics; separation techniques

Received 20 January 2013; accepted 1 August 2013
DOI: 10.1002/app.39801

INTRODUCTION

Water pollution caused by toxic heavy-metal ions, such as Cu^{2+}, Pb^{2+}, and Cd^{2+}, from aqueous solution and industrial wastewater has become a hot topic and is challenging researchers and engineers.[1–4] Generally, these toxic heavy-metal ions cannot be effectively biodegraded in nature and are easily accumulated in the human body and other organisms. It has been reported[5] that an excess intake of toxic heavy metals will induce various diseases and health problems in humans. For example, excess intake of Cu^{2+} ions by humans will cause gastrointestinal distress, even liver or kidney damage. Excess intake of Pb^{2+} ions will induce kidney problems or high blood pressure in adults and delays in the physical and mental development of infants and children. Consequently, the removal of heavy-metal ions from an aqueous medium has become an important and urgent issue.

To remove or delete toxic heavy-metal ions from the contaminated aqueous medium, various innovative routes have recently been developed.[6–8] Among which, adsorption with functionalized hybrid material as an adsorbent has been considered one of the most effective techniques because these heavy-metal ions can be chemically bonded by inorganic/organic polymer hybrids. Particularly, as a new type of silica-based hybrid material, ethylene diamine tetraacetic acid (EDTA)-modified hybrid materials used as adsorbents have been paid increasing attention.[6,9,10] This is because EDTA is a typical chelating agent for metal ions and has a powerful complexing ability for metal ions in aqueous media. Its grafting on the molecular chains of hybrid materials will supply them with larger adsorption capacities. Meanwhile, such types of hybrid material also exhibit unique structural properties for the adsorption of metal ions on their surface. Therefore, EDTA-modified hybrid materials used as adsorbents indicate promising applications in the removal of heavy-metal ions from aqueous media.

Recently, attempts have been made to prepare functionalized hybrid adsorbents for the removal of toxic heavy-metal ions

from aqueous solutions. Among these materials, zwitterionic hybrids, simultaneously containing both anionic and cationic groups, were studied in our laboratory.[11–16] These hybrids revealed excellent adsorption properties for divalent heavy-metal ions from water.[12–14] Our continuing interest in such types of hybrid adsorbents has stimulated us to do further work. Therefore, to develop a new route for the preparation of zwitterionic hybrid adsorbents and to investigate their adsorption properties for toxic heavy-metal ions, herein, a novel approach for the preparation of EDTA-modified zwitterionic hybrid materials via a sol–gel process is proposed. Compared with the previous articles,[12,13] the novelty of this new approach is that (1) inorganic ingredients silicone and titanate were incorporated into the hybrid matrix via a sol–gel process and (2) EDTA, which was used as a strong chelating agent to capture heavy-metal ions, was introduced into the prepared zwitterionic hybrid materials via the reaction of the carboxylic groups (—COOH) in EDTA with the amino groups ($—NH_2$) in the molecular chains of the hybrid precursors. Moreover, the adsorption behaviors of these zwitterionic hybrid materials for Pb^{2+} ions were examined as a typical model for the removal of toxic divalent heavy-metal ions from aqueous solution.

EXPERIMENTAL

Materials

3-Aminopropyl trimethoxysilane (APTMS) was purchased from Jiangsu Chenguang Coincident Dose Co., Ltd. (Danyang City, China) and was used without further purification. Tetra-*n*-butyl titanate, titanium butoxide [$Ti(OBu)_4$], acetylacetone (acac), disodium salt of EDTA, *n*-butanol (BuOH), and other reagents were of analytical grade and used as received.

Preparation of the EDTA-Modified Hybrid Materials

The preparation of the EDTA-modified hybrid materials could be performed in two steps: (1) the fabrication of the hybrid precursor and (2) the modification of the previously prepared hybrid precursor through EDTA salt. These steps are described briefly as follows.

First, both $Ti(OBu)_4$ and acac [the molar ratio of $Ti(OBu)_4$ and acac was fixed at 1:0.1] were dissolved in a BuOH solution (20 mL) and stirred for additional 2 h to prepare the Ti precursor. Second, the proper Ti precursor and APTMS (the molar ratios of samples A–D are listed in Table I) were dissolved in a BuOH solution and stirred violently for an additional 2 h to prepare the hybrid precursor via a sol–gel process. Subsequently, the previously produced hybrid precursor was dried at 80°C for 6 h to obtain the xerogel. After it was cooled to room temperature, the xerogel was immersed in deionized water for 24 h to purge the unreacted reagents and impurities. This xerogel could be applied as an unmodified sample (i.e., the original sample).

Table I. Molar Ratios of Samples A–D

Sample	APTMS (mmol)	$Ti(OBu)_4$ (mmol)	EDTA-modified
A	1	1	
B	1	1	Yes
C	1	0.5	
D	1	0.5	Yes

To obtain an EDTA-modified sample, the previously prepared xerogel (ca. 5.0 g) was further immersed in an EDTA solution (50 mL, 0.1 mol/dm^3) and agitated strongly for 24 h. Subsequently, the mixed solution was filtered. The filtration residue was rinsed with deionized water three times and dried at 80°C for 24 h. The EDTA-modified sample was thus acquired.

Sample Characterization

Fourier transform infrared (FTIR) spectra of the prepared samples A–D were obtained with a Shimadzu FTIR-8400S spectrometer in the region 4000–400 cm^{-1} at a resolution of 0.85 cm^{-1}.

Both thermogravimetric analysis (TGA) and differential scanning calorimetry (DSC) thermal analyses of the samples were measured with a Netzsch STA 409 PC/PG thermogravimetric analyzer under a nitrogen flow at a heating rate of 20°C/min from room temperature (ca. 17°C) to 400°C.

Surface field emission scanning electron microscopy (FESEM) images were observed with a FESEM instrument (Sirion 200) operated at an accelerating voltage of 5.00 kV.

Adsorption Experiments

Adsorption experiments of samples A–D for lead (Pb^{2+}) ions were carried out in a way described in our previous publications,[11,12,16] in which Pb^{2+} ions were used as the adsorption medium. A typical procedure for Pb^{2+} adsorption onto these samples can be described briefly as follows: around 1.0 g of sample was immersed in 25 mL of 0.1 mol/dm^3 aqueous $Pb(NO_3)_2$ solution for 24 h at pH 5 to conduct a static adsorption experiment (in which no agitating equipment was used during the period of adsorption testing to keep the solution still). Subsequently, the adsorbed sample was taken out and washed with deionized water. Finally, an EDTA solution (0.1 mol/dm^3) was used to determine the adsorption capacity of Pb^{2+} ions (q_{Pb2+}) by titrimetric analysis. To decrease the testing errors, the final results were the mean values of three tests.

The q_{Pb2+} value was calculated with eq. (1):

$$q_{Pb^{2+}} = \frac{(C_0\text{-}C_R)V}{W} \quad (1)$$

where V is the volume of the aqueous $Pb(NO_3)_2$ solution (mL); C_0 (mol/dm^3) and C_R are the concentrations of the initial and remaining $Pb(NO_3)_2$ (mol/dm^3), respectively; and W is the weight of the sample (g).

To select the optimal pH scale for Pb^{2+} adsorption, the initial pH of the solution was first determined, in which the pH value of the solution was adjusted with 0.01 mol/L aqueous NaOH or HCl solution. For the adsorption kinetic studies, the samples were immersed in a 0.1 mol/dm^3 aqueous $Pb(NO_3)_2$ solution for different adsorption times at pH 5. Meanwhile, the adsorption isotherm was obtained through changes in the initial concentration, which ranged from 0.01 to 1.0 mol/dm^3, for 24 h at pH 5.

Moreover, the desorption efficiency (percentage) of samples A–D was measured by titrimetric analysis with aqueous HCl solution (0.1 mol/dm^3) as a desorbent.

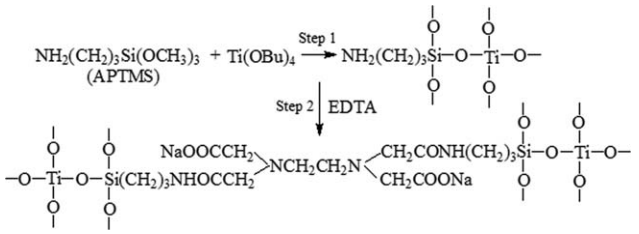

Scheme 1. Formation of the EDTA-modified hybrid materials. In step 1, the alcoholysis and condensation reaction of APTMS and $Ti(OBu)_4$ produced the hybrid precursor. In step 2, the hybrid precursor was further functionalized to create the EDTA-modified hybrid materials.

RESULTS AND DISCUSSION

Preparation of the EDTA-Modified Hybrid Materials

As stated in an earlier section, the preparation procedure for samples A–D could be divided into two steps (see Scheme 1). Step 1 was the alcoholysis and condensation reaction of APTMS and $Ti(OBu)_4$ to produce the hybrid precursor via an Si—O—Ti linkage; step 2 was the further functionalization of the hybrid precursor with EDTA to create desirable EDTA-modified hybrid materials, in which the primary amino groups (—NH_2) in the molecular chains of the hybrid precursor reacted with the carboxylic groups (—COOH) in the molecular chains of EDTA to produce the —CONH— connection. Because the prepared samples simultaneously contained anion-exchange groups (i.e., secondary amino groups) and cation-exchange groups (i.e., carboxylic groups), we thus categorized them as zwitterionic hybrid materials.

In this new route, the fabrication of zwitterionic groups was differentiated from those in our previous publications.[11–13] In the previous studies, the functionalized groups were mainly established by the ring-opening reaction of a lactone reagent and the steric hindrance effect of phenyl groups[11] or a subsequent reaction with a lactone reagent.[12,13] However, in this study, the ionic groups were directly incorporated into the hybrid materials via a sol–gel reaction. In addition, metal Ti was introduced into these hybrid materials via a sol–gel reaction; this was propitious to the elevation of the thermal stability of the synthesized hybrid materials.

FTIR Spectra

To investigate the reaction product presented in Scheme 1, FTIR spectroscopy was performed and is illustrated in Figure 1.

As shown in Figure 1(a–d), we found that the change trends in the adsorption peaks were similar, except for the increase in peak intensity. The peak at 3450 cm^{-1} was in the range of stretching vibrations from the —OH and —NH groups. The absorption peaks at 2935 cm^{-1} were ascribed to the C—H stretching and C—H bending vibrations of —CH_3 and —CH_2 groups, respectively. The strong absorption peaks at 1660 and 1380 cm^{-1} were in the range of stretching vibrations from —COO^- groups and C—N chains. The band at near 1020 cm^{-1} was ascribed to the Si—O—Si, Si—O—C, and C—O—C stretching vibrations.[17]

When we compared the Figure 1 curves a with b and c with d, we found that the peak intensities of the bands at 1660 and

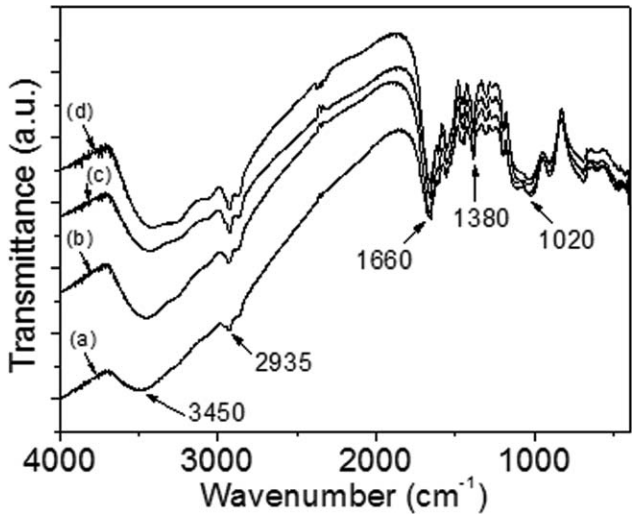

Figure 1. FTIR spectra of samples (a) A, (b) B, (c) C, and (d) D.

1380 cm^{-1} increased remarkably as the sample was modified by EDTA; this implied an increase in the amount of COO^- groups in the modified samples shown in Figure 1(b,d). The reason was assigned to the overlapping of the stretching vibrations from —COO^- groups with C—N stretching band. This observation confirmed the reaction described in Scheme 1 and the existence of —COONa groups in the molecular chains.

TGA Study

Presently, thermal stability is considered an important performance parameter of a hybrid material. Such parameter will impact the application of a hybrid material in some harsh environments. To examine the thermal stability of samples A–D, TGA measurement was performed, and the corresponding graph is illustrated in Figure 2. Meanwhile, the thermal analysis data from the TGA graph are tabulated in Table II.

As presented in Figure 2, we observed that for samples A–D, their change trends in weight loss (percentage) were similar, and two degradation stages could be probed at a weight loss of around 90% (i.e., in the temperature ranges of 40–200 and

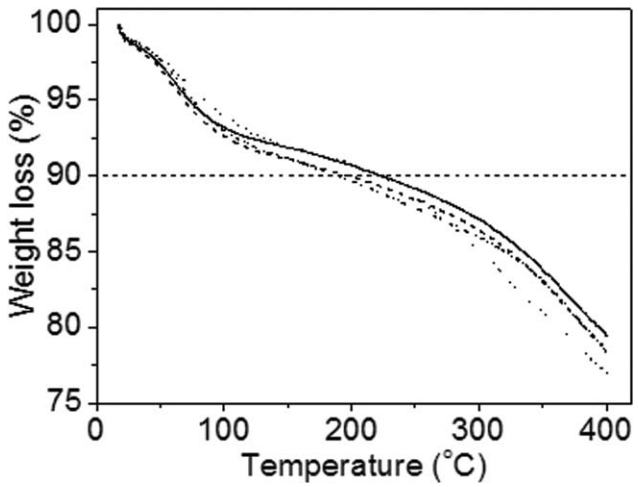

Figure 2. TGA graphs of samples (—) A, (- - -) B, (- · · -) C, and (· · ·) D.

Table II. Thermal Analysis Data for Samples A–D from the TGA Graphs

Sample	T_{d5} (°C)	T_{d10} (°C)	R_{400} (wt %)
A	72.62	224.21	79.36
B	68.66	199.26	78.47
C	75.40	189.83	78.32
D	84.76	221.33	76.92

200–400°C). Accompanying these degradation processes, two exothermic peaks were found in the DSC plot of samples A–D (cf. Figure 3). The first weight loss in the temperature range of 40–200°C was the evaporation of solvents and the degradation of organic ingredients. The second weight loss higher than 200°C was the breakage of functionalized groups and the further formation of the hybrid network.

In addition, it is also shown in Figure 2 that the degradation temperatures at weight losses of 5 and 10% (T_{d5} and T_{d10}, respectively) exhibited various change tendencies. For samples A and B, their T_{d5} and T_{d10} values all displayed downward trends; this implied that the thermal stability of sample A decreased a little after it was modified with EDTA. However, both the T_{d5} and T_{d10} values of samples C and D all revealed upward trends; this suggested that the thermal stability of sample C was elevated slightly as it was modified by EDTA (cf. Table II). These results demonstrate that the addition of $Ti(OBu)_4$ into the previously prepared zwitterionic hybrid materials adjusted their thermal stabilities, and the excess incorporation of $Ti(OBu)_4$ into the hybrid matrix reduced their thermal stability. Furthermore, as shown in Figure 2, the weight loss (percentage) of samples A–D increased quickly as it was larger than 90% (i.e., the degradation temperature value surpassed T_{d10}); this showed that the degradation process was accelerated. This was ascribed to the decomposability of organic ingredients in the high-temperature conditions.

Moreover, as shown in Figure 2, the residual weight at 400°C (R_{400}; weight percentage) indicated a downward trend from samples A to D (cf. Table II). Such downward trend was consistent with the theoretical estimation and was logical when the $Ti(OBu)_4$ content in these samples was considered. Currently, it is accepted that the higher the amount of inorganic additive in a hybrid material is, the higher the remainder in the sintered powder will be. In samples A–D, the $Ti(OBu)_4$ content in them was reduced from sample A to D (see Table I); the amount of sintered powder was thus decreased. Therefore, their change trends in residual weight (weight percentage) were reasonable.

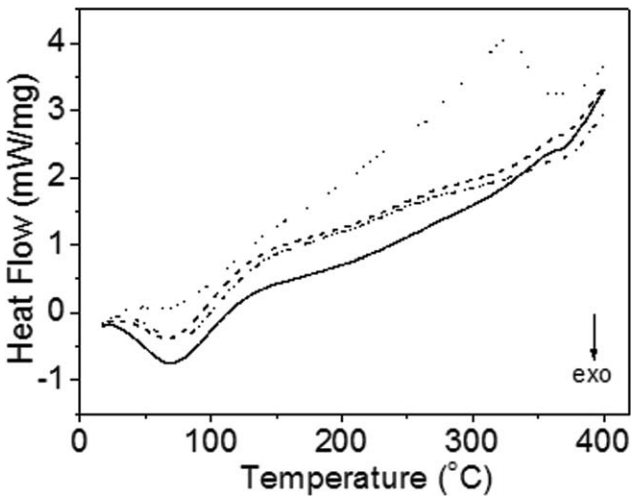

Figure 3. DSC graphs of samples (—) A, (- - -) B, (- · · -) C, and (· · ·) D.

On the basis of the previous findings, we concluded that the thermal stability and amount of remainder in the zwitterionic hybrid materials could be effectively controlled through the proper addition of inorganic species into the hybrid matrix.

DSC Analysis

DSC thermal analysis is a helpful measuring technique in determining the situation of endothermic or exothermic peaks in the DSC curves and the corresponding crystallization performances of a hybrid material. To gain insight into the crystallization transformation of samples A–D, DSC analysis was performed, and the related graph is illustrated in Figure 3. Meanwhile, the peak temperature in the DSC curves is listed in Table III.

As exhibited in Figure 3, for samples A–D, their change trends in the exothermic peak were identical, and two exothermic peaks (i.e., a large exothermic peak below 80°C and a weaker one beyond 360°C) were probed. Meanwhile, we also noted that no endothermic peak was observed in the DSC curves of samples A–C but there was one in that of sample D. Taking sample D taken into account, we found that the trend in the endothermic and endothermic peaks was clearly different from those of samples A–C. Namely, there existed two exothermic peaks (i.e., a weaker exothermic peak below 80°C and a broader one beyond 360°C) and one large endothermic peak at 327°C in the DSC curve of sample D. It was reported[18] that in DSC curves, single or multiple endothermic peaks are the crystal melting, whereas the exothermic peak can be considered as the crystallization. On the basis of this result, we deduced that the melting temperature of sample D was 327°C. In addition, with samples A–D taken into consideration, the first crystallization temperatures (T_{c1}'s; i.e., the first exothermic peak) were situated at 71, 67, 77, and 70°C (cf. Table III), respectively; this showed a downward trend from samples A to B and C to D. Such a trend showed that the T_{c1} value of the EDTA-modified sample was slightly reduced. Furthermore, we discovered that the second crystallization temperatures (T_{c2}'s; i.e., the second exothermic peak) were placed at 366, 370, 372, and 364°C (see Table III). Clearly, the change trend in T_{c2} was in disagreement with that

Table III. Peak Temperatures of Samples A–D from the DSC Curves

	Exothermic peak (°C)		Endothermic peak (°C)
Sample	First	Second	
A	71	366	
B	67	370	
C	77	372	
D	70 (weaker)	364 (larger)	327

of T_{c1}; this demonstrated the influence of the $Ti(OBu)_4$ additive on the crystallization transformation of these samples. The reason was an increase in the hydrophilicity of the EDTA-modified sample due to the grafting of EDTA onto the molecular chains of the hybrid precursor, as described in Scheme 1.

FESEM Images

It is well accepted that for a nonionized material (e.g., activated carbon), the effect of the surface area on the adsorption of heavy-metal ions is distinct.[19] However, for a material containing ionic groups, the effect of the surface area on the adsorption of heavy-metal ions is less important. In our previous study,[11] we found that the surface area of the samples had little impact on the adsorption of heavy-metal ions on the hybrid materials containing ionic groups. Similar results were also seen in other studies.[20,21] To further confirm the influence of the pore size and to examine the surface morphology of the previously prepared zwitterionic hybrid materials, the surface FESEM image of samples A–D were observed and are presented in Figure 4.

As shown in Figure 4(a–d), the surface morphology of the unmodified sample (i.e., the original sample) and the EDTA-modified sample indicated different pore structures. For example, many round particles were uniformly distributed on the surface of the unmodified sample A (i.e., the original sample), and the space among the particles was larger [cf. Figure 4(a)]. Meanwhile, we also noted that many tiny pores were asymmetrically scattered on the surface of sample C when the magnification of the FESEM image was increased up to 40,000× [as illustrated in Figure 4(c)]. In contrast, the particle size of sample B was markedly decreased, and the space among the particles was highly shortened [cf. Figure 4(b)]. A similar observation was also made from the surface of the EDTA-modified sample D, even when the magnification of the FESEM image was increased up to 20,000× [see Figure 4(d)]. These findings revealed that the EDTA modification favored the integration of organic and inorganic moieties, and this led to a decrease in the pore size of the particles.

To explain such trends in the surface morphologies of the samples, please set our eyes on the changes in the hydrophilicity of the previously prepared zwitterionic hybrid materials. Considering the unmodified sample (i.e., original sample) containing weak amino groups (—NH_2 groups) in its molecular chains, its hydrophilicity was relatively weaker; it was thus hard for the solvent to penetrate the tighter surface of the particles. As a result, only small pores were produced on the surface layer [as observed in Figure 4(c)]. When the EDTA-modified sample was taken into account, its hydrophilicity was highly elevated because some strong hydrophilic groups (—COONa groups) were grafted onto the molecular chains, and they indicated a completely acidic dissociation state. Meanwhile, because of the weaker acidic properties and partial dissociation of —COOH groups, the —COONa groups were easily changed into —COOH groups in aqueous solution. Thus, the hybrid matrix was more easily produced under these conditions. Accordingly, both the pore size and particle space of the samples were distinctly decreased.

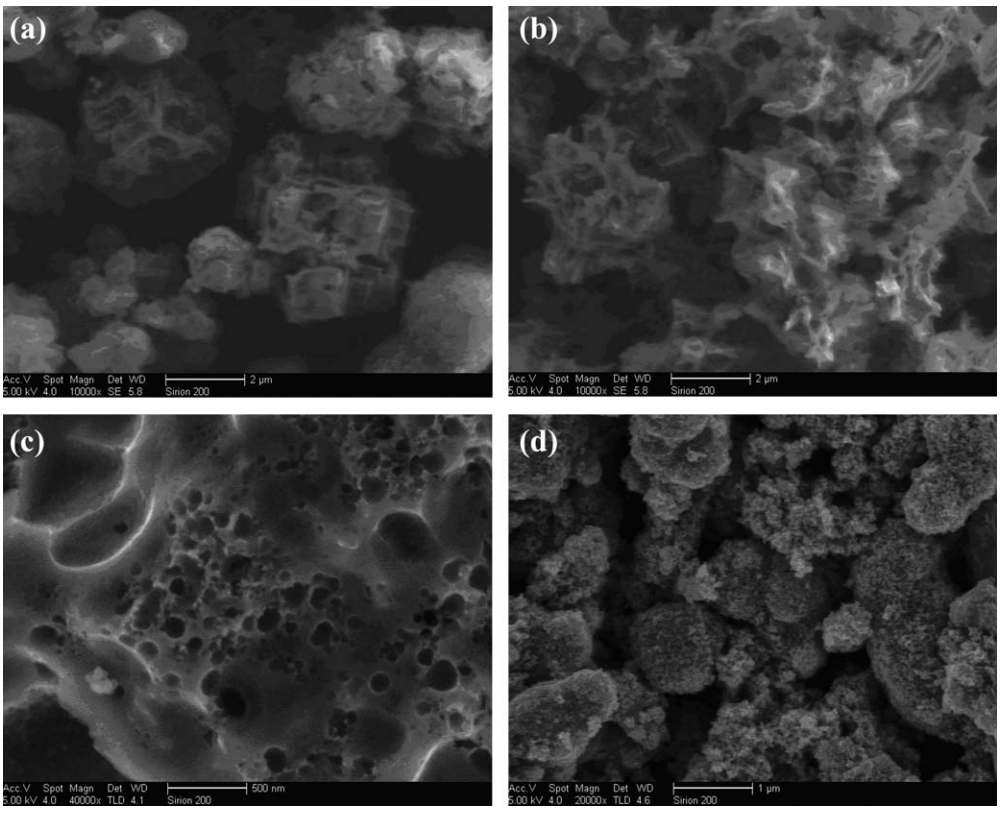

Figure 4. Surface FESEM images of samples (a) A, (b) B, (c) C, and (d) D.

Adsorption of the Pb^{2+} Ions

To better understand the adsorption properties of the EDTA-modified zwitterionic hybrid materials for metal ions in water, adsorption experiments were conducted with Pb^{2+} ions as a typical model of toxic heavy-metal ions. Some dominating influencing factors, such as the initial pH, contact time, and initial solution concentration, were examined. To study the adsorption kinetics and isotherm properties of the Pb^{2+} ions on these zwitterionic hybrid adsorbents, the experimental data were correlated with some two-parameter models, such as the Lagergren pseudo-first-order and pseudo-second-order kinetic equations, intraparticle diffusion model, and Langmuir and Freundlich isotherm equations.

Effect of the Initial pH. The initial pH of the solution had a significant impact on the adsorption of heavy-metal ions onto the hybrid materials; this was because the metal ions could produce sediment in solution as the pH value was elevated to a higher level. To gain the optimal pH value for Pb^{2+} adsorption, the pH in the range of 3–6 at a concentration of 0.1 mol/dm^3 for 24 h was selected to examine effect of the initial pH on Pb^{2+} adsorption. Figure 5 illustrates the effect of the initial pH on Pb^{2+} adsorption.

As shown in Figure 5, q_{Pb2+} of samples A–D increased with the elevated initial pH and reached its highest value at pH 5. Followed, q_{Pb2+} on samples A–D decreased when the initial pH was higher than 5. On the basis of this result, aqueous $Pb(NO_3)_2$ solution at pH 5 was thus chosen as the adsorption medium to study the adsorption behaviors of Pb^{2+} ions onto the prepared zwitterionic hybrid materials.

It should be mentioned that by comparison with the previous jobs,[11,12] we observed that the initial pH in this case was slightly higher than that used in a previous study,[11] in which hybrid adsorbents simultaneously containing —COOH and —NH— groups were used to remove Pb^{2+} ions in pH 4 solution conditions, but similar to that preformed in a previous job,[12] in which the zwitterionic hybrid polymers simultaneously containing —COOH and —COO^- groups and —N^+— groups were applied to remove Pb^{2+} ions in a pH 5 aqueous medium. A similar result was reported in a newly published article.[22] Nava et al.[22] reported that the maximum Pb (II) adsorption was also located in the pH range 5–6 with hybrid adsorbents functionalized with —NH_2 groups. This stability in the initial pH range induced a comparison of the adsorption capacity obtained from different hybrid adsorbents.

Adsorption Kinetics. The relationship of q_{Pb2+} as a function of the contact time t (hours), that is, the adsorption kinetic curves of Pb^{2+} ions on samples A–D, is presented in Figure 6. The time range of kinetic experiments was within 0–18 h. As shown in Figure 6, the q_{Pb2+} values for samples A–D increased with the elapsed contact time. However, taking the individual sample into account, we detected various change trends. For example, when we compared the q_{Pb2+} value of samples A and B, we found that the q_{Pb2+} of sample B (i.e., the EDTA-modified sample) was lower than that of sample A (i.e., the original sample) when the testing error was ignored. Meanwhile, we also found that the q_{Pb2+} of sample D (i.e., the EDTA-modified sample) was higher than that of sample C (i.e., the original sample). This finding suggested that the proper addition of the inorganic composition $Ti(OBu)_4$ into the hybrid polymer favored Pb^{2+} adsorption onto the sample. However, excess incorporation of the inorganic composition $Ti(OBu)_4$ into the hybrid material did not increase the adsorption capacity for heavy-metal ions.

Notice that the change trends in q_{Pb2+} were consistent with those in the thermal stability of the samples found in the TGA curves; this demonstrated that addition of $Ti(OBu)_4$ into the EDTA-modified zwitterionic hybrid materials not only impacted their thermal stabilities but also influenced their adsorption behaviors for Pb^{2+} ions.

It is well known that the Lagergren kinetic equation is a useful model for describing the adsorption properties of a species.[23,24] The Lagergren pseudo-first-order and pseudo-second-order kinetic equations can be linearly expressed as eqs. (2a) and (2b), respectively:

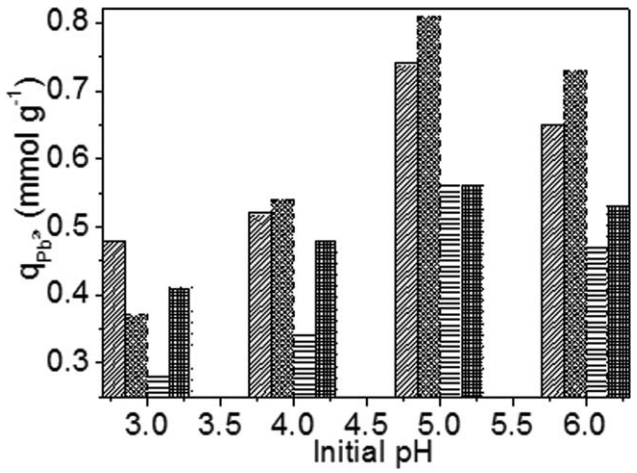

Figure 5. Initial pH versus q_{Pb2+} on samples A (filled with diagonal line), B (filled with diagonal mesh), C (filled with horizontal line), and D (filled with cross grid).

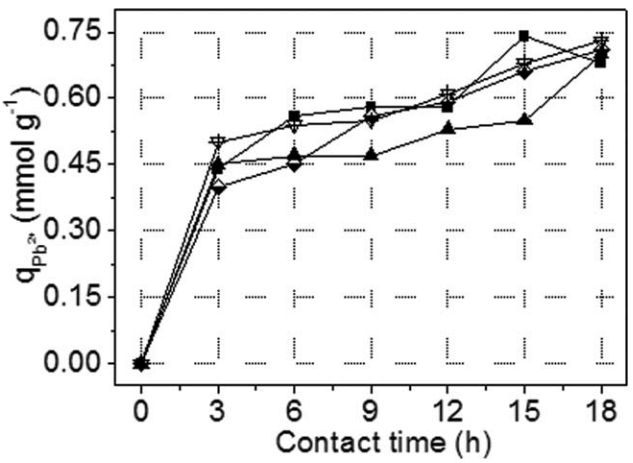

Figure 6. Adsorption kinetic curves of the Pb^{2+} ions on sample A (■), sample B (half-down diamond), sample C (▲), and sample D (▼). The concentration of the aqueous $Pb(NO_3)_2$ solution was 0.1 mol/dm^3 at pH 5.

$$q_t = q_e(1-e^{-k_1 t}) \quad (2a)$$

or

$$\log(q_e - q_t) = \log q_e - \frac{k_1}{2.303} t \quad (2b)$$

$$q_t = \frac{q_e^2 k_2 t}{(1+q_e k_2 t)} \quad (3a)$$

or

$$\frac{t}{q_t} = \frac{1}{k_2 q_e^2} + \frac{t}{q_e} \quad (3b)$$

where k_1 (h^{-1}) and k_2 (g h^{-1} $mmol^{-1}$) are the pseudo-first and pseudo-second-order rate constants, respectively, and q_t (mmol/g) and q_e (mmol/g) are the adsorption capacities of the metal ions (Me^{2+}) at time t and in the equilibrium state, respectively.

The Lagergren adsorption kinetic model for Pb^{2+} adsorption onto samples A–D was calculated and is exhibited in Figure 7(a,b). The linear regression coefficient (R^2) of the Lagergren pseudo-first-order model showed a worse fit for Pb^{2+} adsorption onto samples A–D ($R^2 < 0.9$, cf. Table IV). On the contrary, the Lagergren pseudo-second-order model had a better R^2 for Pb^{2+} adsorption onto samples A–D ($R^2 > 0.9$, see Table IV). This result demonstrated that Pb^{2+} adsorption onto these zwitterionic hybrid materials followed the Lagergren pseudo-second-order kinetic model.

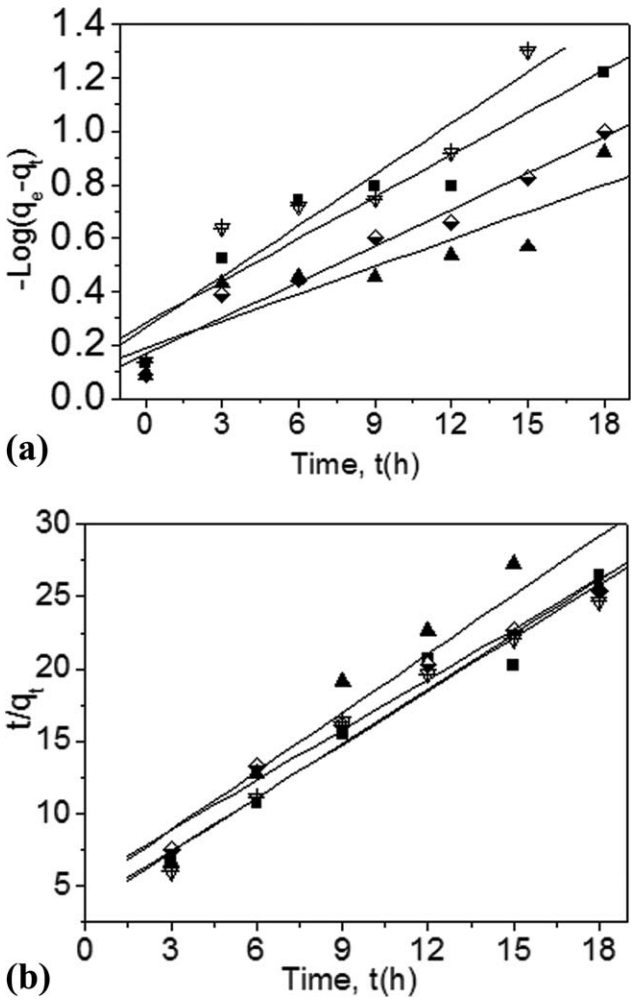

Figure 7. Lagergren kinetic model for Pb^{2+} adsorption onto sample A (■), sample B (half-down diamond), sample C (▲), and sample D (▼): (a) first-order model and (b) second-order model.

In a comparison with previously studies,[11,12] we found that although Pb^{2+} adsorption onto these hybrid adsorbents followed the Lagergren pseudo-second-order kinetic model, the difference in k_2 was distinct. For example, the k_2 values in this case were lower than those reported in our previous articles;[11,12] this suggests that the incorporation of titanium in the hybrid matrix had some influence on the Pb^{2+} adsorption. The possible reason could be ascribed to the orbital structure of titanium. As a reviewer suggested, because titanium has four bonds, their d orbitals are empty (d0) so that this metal could have interfered with the approach of the metal ions to the functional groups present in the hybrid material.

Intraparticle Diffusion. It was reported that when metal ions are adsorbed by an adsorbent, the metal ions transport from the solution through the interface between the solution and the adsorbent into the pores of the particles. Such transport performance of metal ions can be described via the intraparticle diffusion model.[25] To examine the interface transport properties of the Pb^{2+} ions from the interior of the prepared samples, the intraparticle diffusion model was measured. The effect of intraparticle diffusion on the adsorption rate of the Pb^{2+} ions was calculated on the basis of the function relationship of q_t versus t, which can be expressed as eq. (4):[25]

$$q_t = x_i + k_p t^{0.5} \quad (4)$$

where k_p is the intraparticle diffusion rate constant (mmol g^{-1} $h^{-1/2}$) and x_i is the intercept of the straight line, which is related to the boundary layer thickness (mmol/g).

Currently, it is well accepted that if the plot of q_t versus $t^{0.5}$ (the square root of time, t) gives a straight line, the adsorption process is solely controlled by intraparticle diffusion. In contrast, if the experimental data exhibit multilinear plots, two or more steps influence the adsorption process.[25,26]

The intraparticle diffusion curves of Pb^{2+} adsorption onto samples A–D are presented in Figure 8, and the related parameters are listed in Table IV. As shown in Figure 8, we observed that the graph of q_{Pb2+} versus $t^{0.5}$ gave a straight line, and R^2 fit well for Pb^{2+} adsorption onto samples A, B, and D but not sample C. Because the linear lines all nearly passed through the origin of coordinates (i.e., $x_i \approx 0$, cf. Table IV), we thus concluded that Pb^{2+} adsorption onto these samples was solely controlled by intraparticle diffusion.

Notice that this outcome was clearly different from the results obtained in our previous studies,[11,12] in which Pb^{2+} adsorption onto the prepared hybrid adsorbents was not governed by intraparticle diffusion, and diffusion-controlled adsorption mechanisms were the major process. These distinctions in the effect of intraparticle diffusion chiefly arose from the differences in the

Table IV. Kinetic Model Parameters for Pb^{2+} Adsorption

		Pseudo-first-order			Pseudo-second-order			Intraparticle diffusion		
Sample	q^a_{exp}	k_1	q^b_{cal}	R^2	k_2	q^b_{cal}	R^2	k_p	x_i	R^2
A	0.74	0.121	0.523	0.897	0.447	0.794	0.963	0.160	0.0817	0.910
B	0.81	0.104	0.685	0.968	0.249	0.862	0.978	0.162	0.0483	0.973
C	0.82	0.0783	0.649	0.805	0.381	0.738	0.910	0.140	0.0776	0.884
D	0.73	0.146	0.542	0.886	0.410	0.811	0.970	0.158	0.0927	0.906

[a] q_{exp} was the experimental values.
[b] q_{cal} was the calculated values.

hybrid adsorbents containing various ionic groups in the molecular chains.

Moreover, a decrease in the pore size (as presented in Figure 4), and the formation of the hybrid matrix might also have been responsible for the aforementioned trend.

Adsorption Isotherms. Langmuir and Freundlich isotherm equations are two conventional model tools used to examine the adsorption behaviors of metal ions on the interface of a solid material. Generally, the Langmuir isotherm equation is based on monolayer adsorption onto the active reaction sites of the adsorbent and can be expressed as eq. (5):[25,27]

$$\frac{C_e}{q_e} = \frac{C_e}{Q_m} + \frac{1}{Q_m b} \tag{5}$$

where C_e is the equilibrium concentration of metal ions in the liquid phases (mol/dm^3) and Q_m (mmol/g) and b (dm^3/mol) are Langmuir constants, which can be calculated from the intercept and slope of the linear plot based on C_e/q_e versus C_e.

Unlike the surface adsorption from the Langmuir isotherm model, the Freundlich isotherm equation was considered as the adsorption occurred on a heterogeneous surface with uniform energy; this can be expressed with eqs. (6a) and (6b):[25,27]

$$q_e = k_F C_e^{\frac{1}{n}} \tag{6a}$$

$$\log q_e = \log k_F + \frac{1}{n}\log C_e \tag{6b}$$

where k_F [(mmol/g) (mol/dm^3)$^{-1/n}$] and n are the Freundlich constants and can be calculated from the slope and intercept of the linear plot according to log q_e versus log C_e.

The q_{Pb2+} values onto samples A–D versus the initial solution concentration (i.e., adsorption isotherm of the Pb^{2+} ions onto samples A–D) are illustrated in Figure 9. As shown in Figure 9, we found that q_{Pb2+} onto samples A–D increased with the elevated initial solution concentration.

On the basis of Figure 9, the Langmuir and Freundlich isotherm parameters were calculated and are summarized in Table V. As shown in Table V, we observed that that the experimental data fit well with the Langmuir isotherm equation ($R^2 > 0.99$). However, these data fit worse with the Freundlich isotherm equation ($R^2 < 0.90$). This outcome showed that Pb^{2+} adsorption onto these samples was Langmuir monolayer adsorption rather than heterogeneous surface adsorption. This finding in the isotherm model was consistent with the results concluded in the previous studies[11,12] and demonstrated that Pb^{2+} adsorption onto the hybrid adsorbents containing ionic groups was chiefly controlled by the Langmuir model. Furthermore, when we compared the Q_m values in this case with those achieved in previous studies,[11,12] we found that these Q_m values were markedly lower than those obtained previously; this implied that the categories

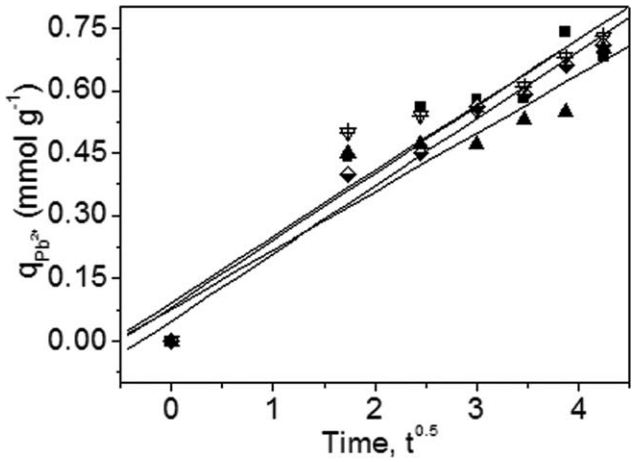

Figure 8. Intraparticle diffusion curves of Pb^{2+} adsorption onto sample A (■), sample B (half-down diamond), sample C (▲), and sample D (▼).

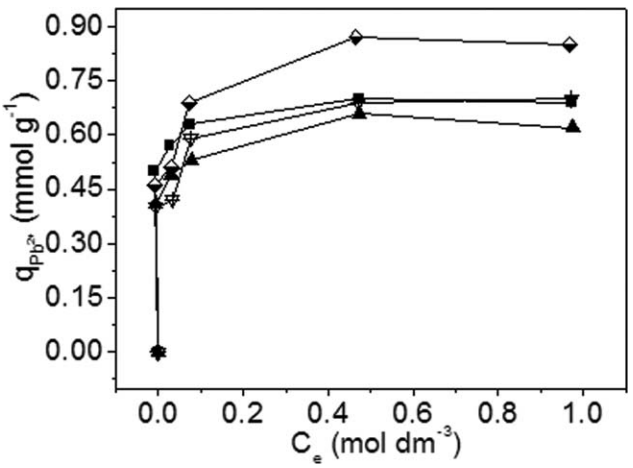

Figure 9. q_{Pb2+} on sample A (■), sample B (half-down diamond), sample C (▲), and sample D (▼) versus C_e.

Table V. Langmuir and Freundlich Isotherm Parameters for Pb^{2+} Adsorption

	Langmuir			Freundlich		
Sample	Q_m	b	R^2	k_F	n	R^2
A	0.693	540.355	0.999	0.710	18.152	0.909
B	0.860	129.337	0.999	0.915	6.979	0.872
C	0.628	525.475	0.998	0.654	12.457	0.867
D	0.707	91.546	0.999	0.742	7.261	0.825

and amounts of ionic groups in the molecular chains were the two dominating factors for Pb^{2+} adsorption. These results were very meaningful in the structural design of hybrid adsorbents.

Moreover, for the Langmuir isotherm model, it was reported[25,27] that the separation factor or equilibrium parameter (R_L) could be used to further examine the favorability of adsorption. When the R_L value is within $0 < R_L < 1$, it is favorable adsorption. Otherwise, it is unfavorable adsorption. The R_L value can be obtained with eq. (7):[25,27]

$$R_L = \frac{1}{(1+bC_0)} \tag{7}$$

where b is the Langmuir equilibrium constant (dm^3/mol).

Table VI lists the calculated R_L values based on the Langmuir isotherm constant. As shown in Table VI, the R_L values of samples A–D were all in the range $0 < R_L < 1$; this suggested that the Pb^{2+} adsorption onto these samples was favorable; this was further confirmed by the Gibbs free energy (ΔG). This finding confirmed that these zwitterionic hybrid materials are promising adsorbents for Pb^{2+} removal from wastewater or contaminated water for environmental application.

ΔG. The calculation of the thermodynamic parameter is of vital importance for the removal of heavy-metal ions via adsorption. It was reported[3] that for the Langmuir adsorption process, ΔG can be calculated with eq. (8):

$$\Delta G = -RT\ln b \tag{8}$$

where R is the gas constant (8.314 J/mol K) and T is the absolute temperature (K).

The ΔG values for the Pb^{2+}-adsorption on samples A–D were calculated and are tabulated in Table VII. As listed in Table VII, the ΔG values were all negative for samples A–D. This result suggested that Pb^{2+} adsorption onto these samples was spontaneous in nature and further corroborated the findings obtained from R_L.

Desorption Experiment

Currently, it is well accepted that regeneration and recovery of spent adsorbents and metals, respectively, are of vital importance for industrial applications of adsorbents.[28] A desorption experiment was thus carried out, and the corresponding data are summarized in Table VIII.

We found that the desorption efficiency (percentage) of these samples with aqueous HCl solution as a desorbent was 20%. This finding suggests that the adsorbed samples could be effective in the regeneration or reuse with aqueous HCl solution as a desorbent and indicated their potential applications in the removal of heavy-metal ions from water.

CONCLUSIONS

A series of zwitterionic hybrid materials, in which EDTA was used as a strong chelating agent to modify ionic groups, were prepared and used to separate Pb^{2+} ions from an aqueous solution. We found that the proper addition of $Ti(OBu)_4$ into these hybrid materials favored their adsorption for Pb^{2+} ions. However, the excess incorporation of $Ti(OBu)_4$ into them did not induce an increase in q_{Pb2+}. These outcomes demonstrate that the adsorption properties of EDTA-modified zwitterionic hybrid materials could be artificially controlled via the incorporation of an inorganic composition. In addition, the adsorption experiments confirmed that Pb^{2+} adsorption followed the Lagergren pseudo-second-order kinetic model, intraparticle diffusion, and Langmuir isotherm model, and they could be reused with aqueous HCl solution as a desorbent.

Table VI. Calculated R_L Values Based on the Langmuir Isotherm Constant

	R_L value			
C_0 (mol/dm^3)	A	B	C	D
0.01	0.156	0.436	0.159	0.522
0.05	0.0356	0.133	0.0366	0.179
0.1	0.0181	0.0717	0.0186	0.0984
0.5	0.00369	0.0152	0.00379	0.0213
1.0	0.00185	0.00767	0.00190	0.0108

Table VII. Calculated ΔG Values at 25°C

Sample	Temperature (K)	ln b	ΔG (kJ/mol)
A	298.15	6.292	−15.597
B	298.15	4.862	−12.053
C	298.15	6.264	−15.528
D	298.15	4.516	−11.196

Table VIII. Desorption Efficiency of Samples A–D for Pb^{2+} Ions

Sample	HCl concentration (mol/dm^3)	Desorption time (h)	Efficiency (%)
A	0.1	5	23.58
B	0.1	5	18.18
C	0.1	5	19.95
D	0.1	5	20.76

ACKNOWLEDGMENTS

This project was financially supported in part by the National Natural Science Foundation of China (contract grant number 21076055), the Significant Foundation of the Educational Committee of Anhui Province (contract grant number ZD2008002-1), the Second National-Level College Students' Innovative Entrepreneurial Training Plan Program (contract grant number 201210878050), and the Science and Technology Innovation Fund for Students of Anhui Jianzhu University (contract grant number C12069).

REFERENCES

1. Li, J.; Zhang, S. W.; Chen, C. L.; Zhao, G. X.; Yang, X.; Li, J. X.; Wang, X. K. *ACS Appl. Mater. Interfaces* **2012**, *4*, 4991.
2. Abdel-Razik, H. H.; Abbo, M.; Almahy, H. A. *J. Appl. Polym. Sci.* **2012**, *125*, 2102.
3. Karatas, M. *J. Hazard. Mater.* **2012**, *199*, 383.
4. Júnior, O. K.; Gurgel, L. V. A.; Freitas, R. P.; Gil, L. F. *Carbohydr. Polym.* **2009**, *77*, 643.
5. U. S. Environmental Protection Agency. National Primary Drinking Water Regulations (EPA 816-F-09-004); **2009**.
6. Jiang, Y. J.; Gao, Q. M.; Yu, H. G.; Chen, Y. R.; Deng, F. *Micropor. Mesopor. Mater.* **2007**, *103*, 316. Elsevier, the Netherlands.
7. Badruddoza, A. Z. M.; Tay, A. S. H; Tan, P. Y.; Hidajat, K.; Uddin, M. S. *J. Hazard. Mater.* **2011**, *185*, 1177.
8. Alothman, Z. A.; Apblett, A. W. *J. Hazard. Mater.* **2010**, *182*, 581.
9. Huang, J.; Ye, M.; Qu, Y.; Chu, L.; Chen, R.; He, Q.; Xu, D. *J. Colloid Interface Sci.* **2012**, *385*, 137.
10. Repo, E.; Warchoł, J. K.; Bhatnagar, A.; Sillanpää, M. *J. Colloid Interface Sci.* **2011**, *358*, 261.
11. Liu, J. S.; Si, J. Y.; Zhang, Q.; Zheng, J. H.; Han, C. L.; Shao, G. Q. *Ind. Eng. Chem. Res.* **2011**, *50*, 8645.
12. Liu, J. S.; Song, L.; Shao, G. Q. *J. Chem. Eng. Data* **2011**, *56*, 2119.
13. Dong, Q.; Liu, J. S.; Song, L.; Shao, G. Q. *J. Hazard. Mater.* **2011**, *186*, 1335.
14. Hu, K. Y.; Liu, J. S.; Wo, H. Z.; Li, T. *J. Appl. Polym. Sci.* **2010**, *118*, 42.
15. Liu, J. S.; Wang, X. H.; Xu, T. W.; Shao, G. Q. *Sep. Purif. Technol.* **2009**, *66*, 135.
16. Liu, J. S.; Ma, Y.; Xu, T. W.; Shao, G. Q. *J. Hazard. Mater.* **2010**, *178*, 1021.
17. Zhang, S. L.; Xu, T. W.; Wu, C. M. *J. Membr. Sci.* **2006**, *269*, 142.
18. Chang, J.-H.; Park, D.-K.; Ihn, K. J. *J. Appl. Polym. Sci.* **2002**, *84*, 2294.
19. Liu, H.; Dai, P.; Zhang, J.; Zhang, C.; Bao, N.; Cheng, C.; Ren, L. *Chem. Eng. J.* **2013**, *228*, 425.
20. Amoyaw, P.; Ingram, C.; Hsu, F.-L.; Bu, X. R. *J. Appl. Polym. Sci.* **2009**, *113*, 2096.
21. Ge, H. C.; Huang, S. Y. *J. Appl. Polym. Sci.* **2010**, *115*, 514.
22. Hernández-Morales, V.; Nava, R.; Acosta-Silva, Y. J.; Macías-Sánchez, S. A.; Pérez-Bueno, J. J.; Pawelec, B. *Micropor. Mesopor. Mater.* **2012**, *160*, 133.
23. Kumar, G. P.; Kumar, P. A.; Chakraborty, S.; Ray, M. *Sep. Purif. Technol.* **2007**, *57*, 47.
24. Mohan, D.; Singh, K. P. *Water Res.* **2002**, *36*, 2304.
25. Atia, A. A.; Donia, A. M.; Yousif, A. M. *Sep. Purif. Technol.* **2008**, *61*, 348.
26. Guibal, E.; Milot, C.; Tobin, J. M. *Ind. Eng. Chem. Res.* **1998**, *37*, 1454.
27. Wang, J.; Kuo, Y. *J. Appl. Polym. Sci.* **2007**, *105*, 1480.
28. Ramesh, A.; Hasegawa, H.; Maki, T.; Ueda, K. *Sep. Purif. Technol.* **2007**, *56*, 90.